Extracting the anisotropy information of crustal rocks from the seismological garbage

Li-Sheng Xu (xuls@cea-igp.ac.cn)
institute of Geophysics,CEA
Zhang Zhe
Fu Zhen
Chun-Lai Li
institute of Geophysics CEA

Physical Sciences - Article

Keywords:

Posted Date: March 23rd, 2022

DOI: https://doi.org/10.21203/rs.3.rs-1420954/v1

Abstract

Human has been eagerly expecting to know some information that can indicate a large earthquake's impending1,2,3,4,5. Decades of efforts showed that the impending of large earthquakes was usually accompanied by a process of regional weakening manifested with multiple temporal and spatial scaled deformation, and such a deformation was often accompanied by clusters or swarms of micro-earthquakes6, which further caused observable change in anisotropy of nearby rocks7,8,9,10. Here we show that the anisotropy information of crustal rocks may be extracted from the seismological garbage, the travel-time residuals produced by dense seismic stations which record clusters or swarms of micro-earthquakes, by means of a new concept, the slowness deviation tensor expressing 3-axis slowness anisotropy. In particular, we present a real example to justify that the slowness deviation tensor with arbitrarily inclined axis may be successfully extracted from the travel-time residual data, and meanwhile to demonstrate that this anisotropy reflected by the extracted tensor mainly originated from the local stress action or deformation. Undoubtedly, this work provides a completely new methodology to link the clusters or swarms of micro-earthquakes with the weakening process which occur before large earthquakes, which essentially contributes a promising direction toward the information that human has been expecting for.

Background

Large earthquakes often produce huge loss in economy and life, for example, the Mw7.9 earthquake having occurred in Wenchuan, China in 2008 killed more than 90 thousand people and ruined almost all the cities and villages along the over-100km-long seismogenic fault[11,12]. Over a century, geo-scientists have been seeking for the information that indicates impending of large earthquakes[1,2,3,4,5]. Only months ago, a process of regional weakening was proposed as a new model for the generation of large earthquakes, during which temporally and spatially multi-scaled deformation was manifested and characterized with clusters or swarms of micro-earthquakes[6]. This model states that deformation should be the primary information associated with generation of large earthquakes, and micro-earthquakes in styles of clusters or swarms should be the primary manifestation. However, a question was remained: how to build a bridge to physically link the deformation with the manifestation?

For decades, the efforts in seismological and rock-laboratory studies[7,8,9,10] have revealed that micro-earthquake seismicity were able to cause stress change, and deformation were able to produce rock anisotropy. Apparently, using anisotropic property to monitor deformation is a good choice, and the interrelation between deformation and stress change makes it possible to extract anisotropic information by observing micro-seismicity.

The anisotropy of the rocks that make up the Earth is simply divided into two types: the LPO (lattice-preferred orientation) formed by the alignment of intrinsically anisotropic mineral grains, and the SPO (shape-preferred orientation) generated by the ordered assembly of individually isotropic materials, and any of them may lead to a speed difference of up to and even exceeding 10% for the waves of different

polarization or propagation directions[13,14]. However, the crust and especially upper crust is almost dominated by the SPO due to the deformation response to long-term stress action[15,16,17,18,19].

Reviewing the works associated with seismic anisotropy, we noticed that in most of them shear waves, instead of compressional waves, were employed [20, 14], and that in a small number of them the inclined symmetrical axis were allowed[21,22,23]. However, compressional waves also contain anisotropy information, and the travel-time measurements of the direct compressional waves are usually more accurate and reliable [24,25]. Moreover, symmetrical axis of anisotropy is generally neither vertical nor horizontal in reality[23,22]. Thus, it will be very significant to extract the information on seismic anisotropy with arbitrarily inclined axis from the direct compressional waves.

Here we present a real example in which we successfully extracted the information on the seismic anisotropy with inclined and vertical axis from a dataset of the travel-time residuals obtained by directly measuring the direct P-wave arrivals of a cluster of micro-earthquakes recorded by a dense seismic array, and in which we adopted an inversion method designed based on a freshly proposed concept, a slowness deviation tensor (SD tensor) describing seismic anisotropy with arbitrarily inclined symmetrical axis. Also, we exhibit a comparison in direction between the stress field inverted from the focal mechanism solutions of the cluster and the seismic anisotropy resolved by the travel-time residuals, to demonstrate that the seismic anisotropy of crustal rocks even under local stress action was detectable. All of these are strongly suggesting that it will be promising and expectable to monitor the weakening process preceding to large earthquakes by densely observing the micro-earthquake seismicity.

1、a Real Example Of Extracting The Anisotropy Information

On May 18, 2020, a sequence of earthquakes, with an M_S5.0 main-shock, occurred in Qiaojia, Yunnan, China. Coincidently, our seismic array was deployed around the sequence (Fig. 1) so that we obtained perfect and reliable travel-time data. The sequence was located within a relatively small volume of 3km×5km[26] so that it could be taken as a cluster and all the events might be approximated at the same source (Fig. 2).

A total of 165 events were precisely located by 10 nearby stations (Fig.1 and Fig. 2a), so the measurements of travel-time in various azimuths were very sufficient. The 1-D velocity model used to locate the events came from local tomography[27], and was specially examined by man-made earthquakes[28], so the travel-time residuals were considered to contain the substantial part of slowness anisotropy.

In order to extract anisotropy information from travel-time residuals, we proposed an inversion system (Supplementary Information). In this system, seismic anisotropy is linearly related with travel-time residuals by a new concept, slowness deviation (SD) tensor. It is stressed that symmetrical axis may be arbitrarily inclined.

At first, we did not impose any constraints, which means that the symmetrical axis may be arbitrary, and the observed data with large standard deviations were automatically removed, which means that the solution was optimized without any artificial disturbances. As Fig.2a shows, a SD tensor with inclined axis was successfully obtained by inverting the automatically selected travel-time residuals as shown in Fig.2b. The inverted parameters were presented in Table S1. The magnitude of the anisotropy was 9.4%, estimated when the isotropic part of the slowness was 1/6km/s. In this case, 409 observed data, which were automatically selected from the raw dataset containing 891 measurements, were fitted with a correlation coefficient (CC) of 0.98.

Next, we constrained the medial axis (N-axis) to be vertical to ground surface, which means that the slow axis (S-axis) and the fast axis (F-axis) both were kept horizontal, and we still allowed the observed data with large standard deviations to be removed automatically. Repeating the same process as above led to the SD tensor as shown in Fig.3a and the observed data fitting as shown in Fig.3b. The inverted parameters were presented in Table S2. In this case, the magnitude of the anisotropy was 4.4% only, and 431 observed data were fitted with a CC of 0.94. Note, one of the 10 stations was automatically removed, implying the non-negligible incline of the symmetrical axis.

2. Comparison Of The Seismic Anisotropy With The Stress Field

In order to obtain a reliable SD tensor reflecting the seismic anisotropy of the observational region, we randomly selected 700 samples of the 891 travel-time residuals, and repeated the inversion 50 times. The individual solutions were used to outline the uncertainty, and their average was accepted as the best solution (Fig.S1a). By repeating the same process, we obtained the best solution together with its uncertainty in case the N-axis was fixed vertical (Fig.S1b, Tables.S5 and S6). The anisotropy magnitudes with and without the constraint were 5.2% and 9.4%, respectively, which both lied in the interval revealed in previous studies[29,30,14].

In the meanwhile, we obtained the principle directions of the local stress field so as to compare with the anisotropic property of the same region. We had successfully obtained the focal mechanism solutions (FMSs) of 70 relatively large events following the Ms5.0 mainshock (Fig. 1) [26]. Following the same strategy as above, we randomly selected 50 samples of the 70 FMSs, and ran the program MSATSI[31,32] 50 times without any constraints and with the constraint of vertical B-axis, respectively. The best solution and its uncertainty inverted were exhibited in Supplementary Information (Figs.S1c and S1d, Tables. S5 and S6). Substantially, the two solutions identically showed a stress setting similar to that in a broader region[33,34].

Additional tests indicated that both of the solutions (SD tensor and stress tensor) for the observational region were sufficiently stable (Supplementary Information). Comparing the directions indicated by the two tensors, we found an intriguing identity: the T-axis and P-axis corresponded to the S-axis and F-axis, respectively. This identity became more outstanding as the B-axis and N-axis both were constrained to be

vertical (Fig.S1b and Fig.S1d), which strongly suggested that the anisotropy was caused mainly by the stress action in this case though it might be caused by other sources somewhere[35,36].

3. Summary

Our work essentially builds a new link between the cluster or swarms of micro-earthquakes proceeding potential large earthquakes and the deformation taking place during the weakening process prior to the large earthquakes. In comparison to shear-wave splitting, the methodology we proposed here is more straight forward, more open, and practically much easier though shear-wave splitting can also supplies with anisotropy information of crustal rocks. Therefore, our work contributes a more promising approach to monitoring the change in deformation or stress.

However, our method seems to require a highly accurate measurements or observations. We spent efforts to extract anisotropic information from S-wave travel-time residuals, but failed. Carefully analyzing the observed travelling times, we found that their uncertainty ranges would become larger when the S-wave arrivals were added to locate the seismic events (Fig. S2). Very probably, the errors in observed S-wave arrivals and S-velocity model both brought disturbance into the S-wave and even P-wave residual, because the SD tensor inversion could be realized successfully only based on pure P-wave arrivals plus accurately chosen P-velocity model[27,28]. Predictably, S-wave residuals will be usable as soon as the S-arrival pick-ups and the S-velocity model become accurate and reliable.

Although we could not have found a case in which a complete process of deformation preceding a large earthquake was observed and the deformation process was successfully monitored with our method, this work has started a new and promising path to the unknown pre-processes of large earthquakes, or at least introduce a new beam of light into the domains of high-precision seismological observations, recycling seismological garbage, monitoring crustal rock deformation, and among others, which will ultimately light up the dark pre-processes of large earthquakes.

References

1. Suyehiro, S. Difference between aftershocks and foreshocks in the relationship of magnitude to frequency of occurrence for the great Chilean earthquake of 1960. Bull. Seism. Soc. Am. 56, 185_200 (1966).
2. Dodge, D. A., Beroza, G. C. & Ellsworth, W. L. Foreshock sequence of the 1992 Landers, California, earthquake and its implications for earthquake nucleation. J. Geophys. Res. 100, 9865_9880 (1995).
3. Bakun, W.H., Aagaard, B., Dost, B., Ellsworth, W.L., Hardebeck, J. L et al. Implications for prediction and hazard assessment from the 2004 Parkfield earthquake. Nature, 437, 969-974, doi: 10.1038 (2005).
4. Bouchon, M., Karabulut, H., Aktar, M., Ozalaybey, S., Schmittbuhl, J. & Bouin, M.P. Extended nucleation of the 1999 Mw 7.6 Izmit earthquake. Science 331, 877_880 (2011).

5. Kato, A., Obara, K., Igarashi, T., Tsuruoka, H., Nakagawa, S. & Hirata, N. Propagation of slow slip leading up to the 2011 Mw 9.0 Tohoku-Oki earthquake. Science 335, 705_708 (2012).
6. Kato, A. and Ben-Zion, Y. The generation of large earthquakes, Nature Reviews Earth & Environment (2), 26-39. doi.org/10.1038/s43017-020-00108- w (2021).
7. Peacock, S., Crampin, S., Booth D. C. and Fletcher J. B. Shear-wave splitting in the Anza seismic gap, Southern California: temporal variations as possible precursors. J. Geophys. Res. 93: 3339-3356 (1988).
8. Booth, D. C., Crampin, S., Lovell, J. H. and Chiu, J. M. Temporal changes in shear-wave splitting during an earthquake swarm in Arkansas. J. Geophys. Res. Solid Earth 95:11151-11164 (1990).
9. Crampin, S, Booth, D. C., Evans, R., Peacock, S and Fletcher, J. B. Changes in shear wave splitting at Anza near the time of the North Palm Springs Earthquake. J. Geophys. Res. 95:11197-11212 (1990).
10. Crampin, S., Peacock, S., Gao, Y. and Chastin, S. The scatter of time delays in shear-wave splitting above small earthquakes. Geophys. J. Int. 156:39-44 (2004).
11. Kerr, R.A. and Stong, R. A human trigger for the great quake of Sichuan? Science, 323(5912): 322. Doi:10.1126/science.323.5912.322 (2009).
12. Zhang, Y., Feng, W. P., Xu, L.S., Zhou, C.H and Chen, Y.T. Spatiao-temporal rupture process of the 2008 great Wenchuan earthquake. Sci.China. Ser D-Earth Sci, 52(2): 145~154 (2009).
13. Plomerova, V. and Plomerova, J. Regional fabric of the deep lithosphere in central Europe from seismic anisotropy. Stud. Geophys. Geod., 39: 219-226(1995).
14. Zhao, D.P., Yu, S. and Liu, X. Seismic anisotropy tomography: New insight into subduction dynamics. Gondwana Research 33: 24–43 (2016).
15. Crampin S, Evans R and Atkinson B K. Earthquake prediction: a new physical basis. Geophys. J. Roy. Astr. Soc. 76: 147-156 (1984).
16. Crampin, S. The fracture criticality of crustal rocks. Geophys. J. Int. 118:428-4381994 (1994).
17. Zatsepin, S.V. and Crampin, S. Modeling the compliance of crustal rock: I-Response of shear-wave splitting to differential stress. Geophys. J. Int. 129:477-494 (1997).
18. Crampin, S. Calculable fluid-rock interactions. J. Geol. Soc. 156:501-549 (1999).
19. Crampin, S. and Chastin, S. A review of shear wave splitting in the crack-critical crust. Geophys. J. Int., 155, 221–240 (2003).
20. Gupta, H. K.(ed.). Encyclopedia of Earth Sciences Series. Published by Springer. P. O. Box 17, 3300 AA Dordrecht. Netherlands. 1-1578 (2011).
21. Plomerova, J., Sileny, J. and Babuska, V. Joint interpretation of upper-mantle anisotropy based on teleseismic P-travel time delays and inversion of shear-wave splitting parameters. Physics of the Earth and Planetary Interiors 95, 293–309 (1996).
22. Plomerova, J., Vecsey, L. and Babuska, V. Domains of Archean mantle lithosphere deciphered by seismic anisotropy - Inferences from the LAPNET array in northern Fennoscandia. Solid Earth 2, 303–313 (2011).

23. Babuska, V. and Plomerova, J. European mantle lithosphere assembled from rigid microplates with inherited seismic anisotropy, Phys. Earth. Planet. Inter., 158, 264–280 (2006).
24. Kennett, B. and Engdahl, E.R. Traveltimes for global earthquake location and phase identification, Geophys. J. Int., 105, 429–465 (1991).
25. Kennett, B.L.N., Engdahl, E.R. and Buland, R. Constraints on seismic velocities in the Earth from travel times, Geophys. J. Int., 122, 108–124 (1995).
26. Fu, Z., Jiang, C., Yin, F.L., Zhang, L., Shen, X.L., Fang, L.H., Li, C.L., Zhang, X. and Xu. L.S. Preliminary Report on the 18 May 2020 Ms 5.0 Qiaojia Earthquake, Yunnan, China, Seismol. Res. Lett. 92, 2122–2133, doi: 10.1785/0220200233 (2021).
27. Wang, C. Y., Chan, W.W. and Mooney, W.D. Three-dimensional velocity structure of curst and upper mantle in southwestern China and its tectonic implications. J. Geophys. Res., 108(B), doi: 10.1029/2002JB001973 (2003).
28. Xu, L.S.，Yan, C., Zhang, X. and Li, C. L. A Method for Determination of Earthquake Hypocentroid: Time-reversal Imaging Technique - An examination based on people-made earthquakes，Chinese J. Geophys. 2013，56(12)，56，12，，4009-4027, doi: 10.6038/cjg20131207 (2013).
29. Christensen, N.I. The magnitude, symmetry and origin of upper mantle anisotropy based on fabric analyses of ultramafic tectonites. Geophysical Journal of the Royal Astronomical Society 76, 89–111 (1984).
30. Babuska, V. and Plomerova, J. Regional fabric of the deep lithosphere in central Europe from seismic anisotropy. Stud. Geophys. Geod., 39: 219-226 (1995).
31. Lund, B., and Townend, J. Calculating horizontal stress orientations with full or partial knowledge of the tectonic stress tensor, Geophys. J. Int. 170, 1328-1335, doi: 10.1111/j.1365-246X.2007.03468.x (2007).
32. Martínez-Garzón, P., Kwiatek, G., Ickrath, M. and Bohnhoff, M. MSATSI: A MATLAB package for stress inversion combining solid classic methodology, a new simplified user-handling and a visualization tool, Seismol. Res. Lett. 85, no. 4, doi: 10.1785/0220130189 (2014).
33. Luo, J., Zhao, C. P., Lv, J., Zhou, L. Q and Zheng, S. H. Characteristics of Focal mechanisms and the stress field in the southeastern margin of the Tibetan Plateau, Pure Appl. Ceophys., doi: 10.1007/s00024-016-1350-8 (2016).
34. Hu, X. P., Zang, A., Hedbach, O., Cui, X. F., Xie, F. R. and Chen, J. W. Crustal stress pattern in China and its adjacent areas, J. Asian Earth Sci., doi: 10.1016/j.jsceaes.2017.07.005 (2017).
35. Crampin, S. and Peacock, S. A review of the current understanding of shear-wave splitting and common fallacies in interpretation, Wave Motion, 45, 675–722(2008).
36. Gao, Y., Wu, J., Fukao, Y., Shi, Y. and Zhu, A. Shear-wave splitting in the crust in North China: stress, faults and tectonic implications, Geophys. J. Int., 187(2), 642–654 (2011).
37. Maupin, V., Park, J. Theory and observations: wave propagation in anisotropic media. In: Schubert, G. (Ed.), Treatise on geophysics. Elsevier, Amsterdam, pp. 289–321 (2007).

38. Browaeys, J. and Chevrot, S. Decomposition of the elastic tensor and geophysical applications. Geophysical Journal International, 159, 667–678 (2004).
39. Crampin, S. The fracture criticality of crustal rocks. Geophys J Int 118:428-438 (1994).

Declarations

Acknowledgements

We thank Profs. Gao Yuan, Li Yonghua and Chang Lijun for their helps. This work is supported by the National Nature Science Foundation of China (U2139205&U2039208).

Author Contributions:

XULS: funding acquisition, conceptualization, methodology, manuscript writing; ZHANGZ: calculation, visualization, review; FUZ: calculation, method, review; LICL: Calculation.

Competing interests:

Authors declare that they have no competing interests

Additional Information:

Supplementary Information is available for this paper.

Correspondence and requests for materials should be addressed to Xu Lisheng (xuls@cea-igp.ac.cn; 1785216234@qq.com)

Figures

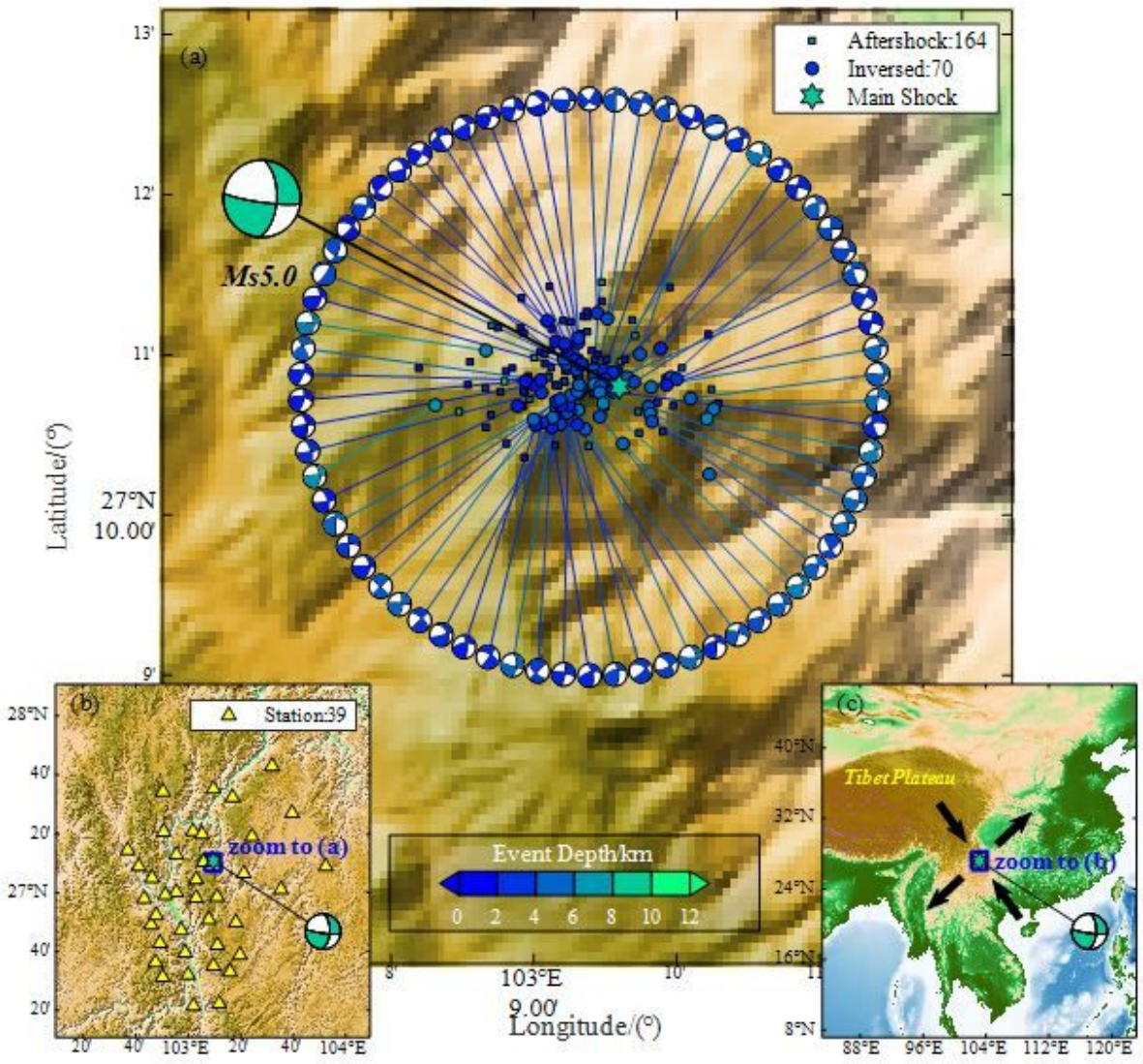

Figure 1

2020 Ms5.0 Qiaojia earthquake sequence and seismic stations. (a) 2020 Ms5.0 Qiaojia earthquake sequence, the main-shock plus its 164 aftershocks, where beach balls denote the focal mechanism solutions of relatively large events; (b) Stations and area of main plot (a); (c) Location of subplot (b) with respect to Tibetan plateau, where arrows show stress-field directions.

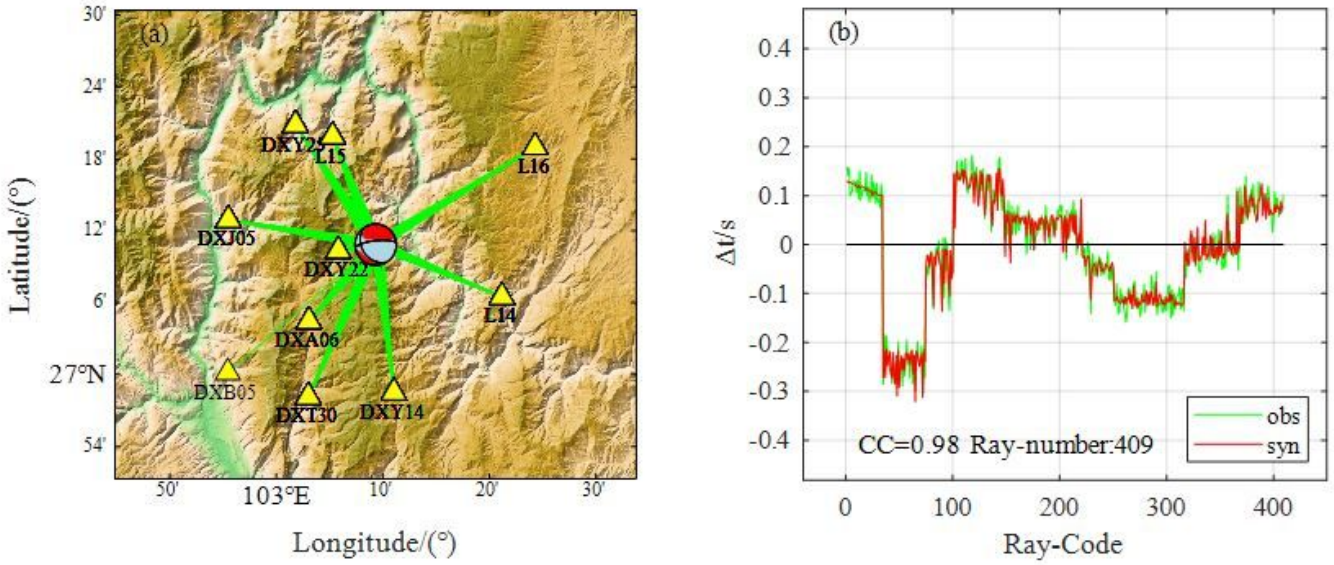

Figure 2

The SD tensor inversion without any constraints. (a) SD tensor (beach ball), stations (yellow triangles) and ray paths (green lines); (b) Comparison of the observed with synthetic data.

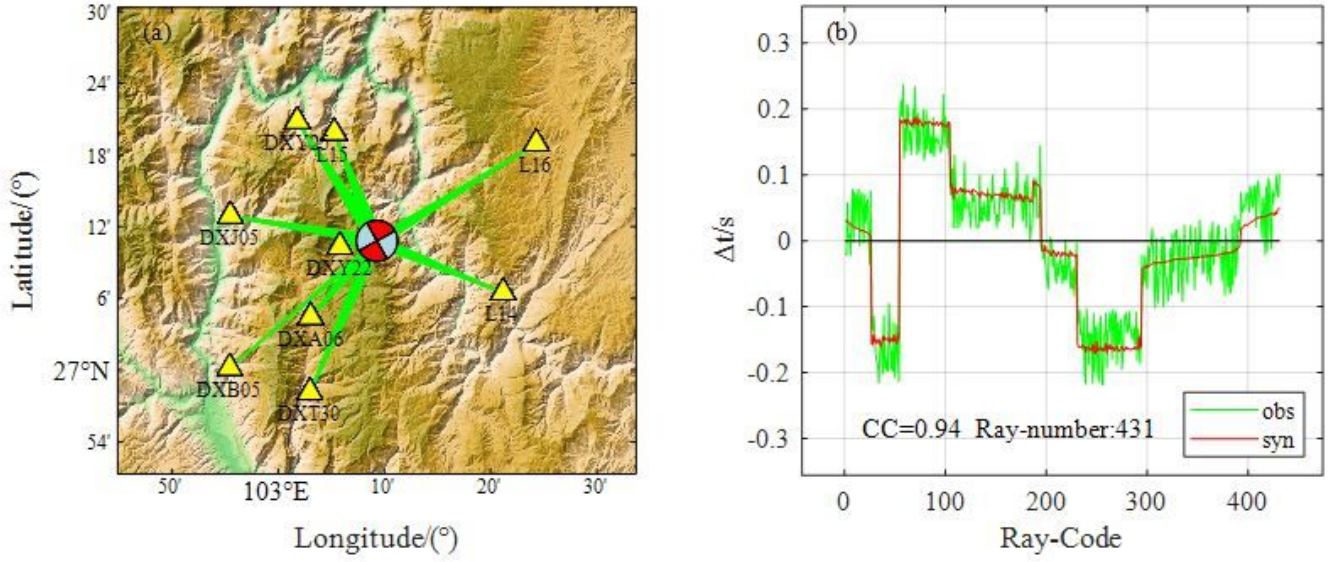

Figure 3

The SD tensor inversion as N-axis was constrained vertical to ground surface. (See Fig.2)

Supplementary Files

This is a list of supplementary files associated with this preprint. Click to download.

- SI20220305.docx